Environmental Science
Processes & Impacts

Unrecognized Volatile and Semi-Volatile Organic Compounds from Brake Wear

Journal:	*Environmental Science: Processes & Impacts*
Manuscript ID	EM-ART-01-2024-000024.R1
Article Type:	Paper

Unrecognized Volatile and Semi-Volatile Organic Compounds from Brake Wear

V. Perraud,[1]† D. R. Blake,[1]† L. M. Wingen,[1] B. Barletta,[1] P. S. Bauer,[1] J. Campos,[2] M. J. Ezell,[1] A. Guenther,[2] K. N. Johnson,[1] M. Lee,[1] S. Meinardi,[1] J. Patterson,[2] E. S. Saltzman,[2] A. E. Thomas,[1] J. N. Smith[1]* and B. J. Finlayson-Pitts[1]*

[1]Department of Chemistry, University of California, Irvine, CA 92697
[2]Department of Earth System Science, University of California. Irvine, CA 92697

†These authors contributed equally to this work
*Corresponding authors

Revisions for Environmental Sciences: Processes and Impacts

March 27, 2024

Electronic Supplementary Information includes

Materials and Methods

Figs. S1-S13

Tables S1-S7

References

Environmental Significance

To mitigate climate change and improve air quality, conventional combustion-powered vehicles are being replaced by zero tailpipe emissions vehicles. We show that in addition to well-documented emissions of particles, automotive braking also emits a complex mixture of volatile organic gases that include Hazardous Air Pollutants, climate active species and gases known to participate in the degradation of air quality. Thus, vehicles will continue to contribute to air quality and climate problems once tailpipe emissions are eliminated.

Abstract

Motor vehicles are among the major sources of pollutants and greenhouse gases in urban areas and a transition to "zero emission vehicles" is underway worldwide. However, emissions associated with brake and tire wear will remain. We show here that a variety of previously unrecognized volatile and semi-volatile organic compounds, some of which are greenhouse gases or classified as Hazardous Air Pollutants, as well as nitrogen-containing organics, nitrogen oxides and ammonia, are emitted during braking. The distribution and reactivity of these gaseous emissions are such that they can react in air to form ozone and other secondary pollutants with adverse health and climate consequences. Some of the compounds may prove to be unique markers of brake emissions. At higher temperatures, nucleation and growth of nanoparticles is also observed. Regions with high traffic, which are often disadvantaged communities, as well as commuters can be impacted by these emissions even after combustion-powered vehicles are phased out.

Introduction:

The inextricably intertwined issues[1] of air quality and climate change present major threats and challenges globally, especially to vulnerable communities. Since the start of the industrial revolution and the expanding use of fossil fuels, atmospheric concentrations of carbon dioxide and other greenhouse gases (GHG) such as nitrous oxide and methane have increased dramatically.[2,3] As global temperatures rise, extreme weather events such as wildfires are increasing.[4] This has resulted in large episodic emissions of both gases and particles that impact air quality, health and climate.[5-7]

Over the past five decades, tailpipe emissions of particles, volatile organic compounds (VOC) and nitrogen oxides (NO_x) from vehicles have declined dramatically in response to regulations.[8-12] With the urgent need to address climate change, there is a transition underway from the use of fossil fuels in vehicles to what are termed zero emission vehicles (ZEV). For example, both the European Union and California have banned the sale of new gasoline-fueled vehicles starting in 2035. However, these will not truly be ZEV since there will be continued emissions of both particles and gases from brakes and tires, as well as resuspension of road dust; it has been suggested that these vehicles actually be designated *ZEEV* for "*zero exhaust emission vehicles"*.[13]

Indeed, with the dramatic reduction in tailpipe emissions over the years, particle emissions from brakes and tires[13-21] are now thought to be about equal by mass to those from tailpipes[16] in developed regions of the world. These have the potential to impact visibility and climate through scattering incoming solar radiation and altering cloud formation and properties, as well as having deleterious effects on humans and ecosystems.[15,22-29] The impacts of particle emissions fall disproportionately on socioeconomically disadvantaged communities,[30,31] often described as environmental justice (EJ) communities, many of which are in heavily trafficked areas either close to major roadways or large distribution centers that have heavy truck traffic. In addition, commuters will continue to be exposed to these emissions.[32,33] In recent Los Angeles area studies, 21% of the oxidative potential of $PM_{2.5}$ was attributed to brake and tire emissions, and both $PM_{2.5}$ mass and the oxidative potential exposures increased in socioeconomically disadvantaged communities.[24,34]

While there is an accelerating transition to EVs, there is no agreement on the magnitude of the changes in non-exhaust emissions that will result. For example, the use of regenerative braking decreases brake emissions but the heavier weight due to the batteries leads to increased emissions.[13-16,34,35] It is noteworthy that the use of autonomous vehicles is expected to increase these emissions since their algorithms require more frequent braking.[14]

While particles associated with non-tailpipe sources have been characterized in a number of studies,[13-16,36-39] relatively little is known about the gases. The most relevant study is that of Placha et al.[40] who measured gas phase benzene, toluene, ethylbenzene, xylenes, polycyclic aromatic hydrocarbons and total organic carbon along with particle composition during brake wear. These results were also reported for a non-commercial brake pad formulated for their experiments rather than commonly used commercial brake pads.

In this study, we focus on C1-C21 volatile and semi-volatile gases emitted during braking, including probing the relationship between these gas emissions and the associated generation and composition of particles from either ceramic or semi-metallic brake pads used widely in the United States. Given the previous extensive work on particle emissions,[13-16,36-39] we do not include a comprehensive treatment of particles but only those aspects that are correlated with the gas emissions. In addition, a search for potential specific gas markers for brake wear was carried out.

This appears to be the first report of this wide suite of VOC as well as NO_x, which individually or through well-known secondary chemistry, are classified as Hazardous Air Pollutants, are climate-active, or generate a host of pollutants[41] that have deleterious impacts on human health and welfare.[22] These harmful secondary pollutants include ozone (also a GHG), nitric acid and particles.

Materials and Methods:

A custom-built brake dynamometer (Fig. S1A)[42] was used for these experiments. The facility employs a heavy-duty metal working 22” lathe (Lodge & Shipley) to rotate a disc brake system

(rotor), spanning the torques and temperatures found in normal driving conditions. The disc brake caliper is a common model (Kodiak model 225) for which a large variety of brake pads are commercially available. Different compositions of brake pad linings exist and are favored in different international markets. Two representative classes of linings were chosen for this study that were readily available: a ceramic (Kodiak model DBC-225) and a semi-metallic (BrakeBest model MKD289) brake pad. The exact formulation of the linings investigated is confidential and proprietary, but brake pads typically include five crucial common components: friction material, mixed in with binders, fillers, lubricants and reinforcement fibers.[43-46] This results in a complex mixture of organic and inorganic components. Semi-metallic brake pads typically have larger amounts of steel fibers and other metals compared to ceramic brakes[14,47] while the ceramic brakes (i.e. aftermarket non-asbestos organic brakes)[48] are composed of mostly organic materials reinforced with aramid, glass or ceramic fibers.[43] These two brake types are common in the US market.[47]

Braking force was applied using an electric over hydraulic brake actuator (Hydrastar, model HBA-12) and a brake controller (Tekonsha, model PowerTrac), the latter of which was modified to accept computer control of braking force and time. For the braking system, DOT3 brake fluid (O'Reilly, 72120) was used. The brake caliper and rotor were enclosed in an 87 L aluminum chamber to allow for clean purge air to be delivered, isolating emissions from surrounding ambient air. The clean air was provided by a purge air generator (Parker-Balston, model 75-62) and was continuously introduced into the chamber via a side-port at 35 L min^{-1}. Sensors housed inside the chamber included a relative humidity (RH) and temperature sensor (Vaisala, model HPM-44), an infrared non-contact temperature sensor for measuring the temperature the rotor surface (Omega model OS301-HT), a pressure sensor for monitoring the pneumatic fluid pressure (AiM, model MC-327), and a torque sensor for monitoring the torque applied to the brake caliper (Ato, model ATO-TQS-S01). All instruments sampling VOC and particle emissions were connected along a single axis across the bottom section of the chamber front panel as seen in Fig. S1B. Sampling lines were ¼ in. aluminum or copper tubing, except for the whole air sampling (WAS) canister and semi-volatile organic compounds (SVOC) sorbent tubes, which were Teflon. The chamber was thoroughly cleaned to remove all particulate residues prior to each experiment.

The lathe was operated at 173 RPM, corresponding to a driving speed of 18 miles hr^{-1} for a typical 35" passenger vehicle wheel. Rotor rotation occurred without braking for several minutes before the first braking regime was applied (hereafter referred as to '*spinning only*' conditions). The first regime (regime 1) was representative of light braking conditions and the second (regime 2) was representative of heavy braking conditions. In regime 1, brake pressure was maintained at 20-22 psi with a torque of ~120-190 N m, while in regime 2, brake pressure was maintained at ~30-32 psi with a torque of ~200-270 N m. In regime 2, the brake torque tends to decrease as the brake heats up, suggesting the brake pads undergo a loss of friction, known as brake fade.[49,50] In regime 1, rotor temperatures typically increased from room temperature to a maximum temperature of 86-177°C depending on the experiment, while in regime 2 the temperatures were typically higher (ranging from 164-358°C). Light braking (regime 1) is characteristic of urban driving, while heavy braking (regime 2) is characteristic of rural and highway driving.[51] The brake torque and rotor temperatures we achieve in the braking regimes adopted in the present study in general compare well with those reported as typical for some common make and model vehicles.[52] The maximum temperatures reached in each experiment are shown in Table S1. A typical set of these parameters for a given experiment for each brake type is presented in Fig. S2. A separate set of experiments focused on collecting particles for toxicology studies was also performed with the same brakes. For these, it was necessary to run the dynamometer under regime 1 conditions for extended times (3-5 hr) which wore the surface of the brake pads heavily. We report here results from six experiments that were chosen to represent a range of conditions from new to heavily worn brake pads.

Although some test cycles have been developed for brakes and tires,[36,51,53] there is no universally accepted protocol. There are a number of factors that impact emissions, including the velocity when the brakes are first applied, the frequency and duration of braking, and the braking power and deceleration rate. Other factors such as the composition of the brake pads and the use history are important as well. As seen in Figs. 1A and 1C, gas emission is closely related to the rotor temperature, the range of which is covered by both braking regimes studied here. The intent of the present studies was not to mimic the overall emissions from proposed test cycles, but rather to determine whether there are significant gas emissions that have been overlooked, how they

depend on braking conditions, and how they may impact air quality. Once universally accepted braking protocols have been established, the emissions as a function of rotor temperature can be used to estimate gas emissions under more realistic driving habits.

Offline analysis of the C1-C10 gas phase VOC was performed using whole air sampling (WAS) with evacuated canisters followed by multicolumn, multidetector gas chromatography.[54] Multiple samples were collected at discrete regular time intervals during each regime. In addition, proton-transfer reaction mass spectrometry (PTR-MS; Ionicon Analytik, model 8000) was used to capture the real-time evolution of VOC throughout the experiments. Further, Tenax/Carbograph 5 sorbent tubes were also collected at discrete regular time intervals and analyzed for volatile and semi-volatile compounds with volatility ranging from pentane (C5) to heneicosane (C21). Additional gas measurements included carbon monoxide (CO), nitric oxide (NO) and nitrogen dioxide (NO_2) that were performed using two commercial analyzers (ThermoFisher model 48i and 42C respectively). Particle size distributions were recorded using a customed scanning mobility particle sizer described in the Electronic Supplementary Information (ESI) and an aerodynamic particle sizer (TSI Inc., model 3936). For composition, particles were collected on carbon coated copper grids for scanning transmission electron microscopy (STEM) and electron dispersion spectroscopy (EDS). Real-time measurement of submicron particle composition was also achieved using a high-resolution aerosol mass spectrometer (AMS, Aerodyne, Inc.). More details on the measurements can be found in the ESI.

Results and Discussion

Figure 1A shows, for a ceramic brake pad, the rotor temperature, equivalent total VOC, CO, NO and NO_2 for regime 1, characterized in this experiment by brake rotor temperatures of up to 115°C, followed by regime 2 braking conditions. Regime 2 is characterized by a new particle formation event (Fig. 1B) when rotor temperatures spanned from 115-177°C. Similar data for semi-metallic brake pads show that even higher temperatures are reached in regime 2 (Fig. 1C and 1D). Emissions of VOC, CO and NO_x increase dramatically in regime 2 for both brake types. The actual onset of the VOC emissions reported by the PTR-ToF-MS in regime 2 was similar to that of CO, NO and NO_2 as illustrated in Fig. S5. The emissions recorded for the semi-metallic brake pads were systematically delayed compared to those of the ceramic brake

pads. As noted in the experimental section, ceramic brake pad linings are expected to have a higher content of organic material that may be more prone to thermal degradation than that of the semi-metallic brake linings. At the end of each experiment, VOC and other trace gases decline quickly, as soon as braking stops. This results from a combination of the rotor temperature decreasing and a dilution effect as the chamber is being continuously flushed with air. Note that the NOx profiles were temperature dependent, and the semi-metallic brake produces less NO and NO_2 than the ceramic brake (Fig. S6). Emissions during regime 1 (lower rotor temperature) were much smaller than those encountered during regime 2, and dominated by small carbonyls (e.g. acetaldehyde, acetone). However, in order to fully characterize the suite of emissions, we focus hereafter on regime 2 results as the concentrations allowed for a variety of simultaneous accurate measurements of both gases and the associated particles.

Particles. Size distributions in regimes 1 and 2 for ceramic brake pads are shown in Fig. 1B and for semi-metallic pads in Fig. 1D. Relatively few, large (micron-sized) particles are generated under the light braking (regime 1), with their metal content and morphology (Figs. S3 and S4, Table S3) similar to those reported previously.[13-16,34,55,56] As the braking intensity and rotor temperature rise (regime 2), large numbers of small particles ranging in size from a few to several hundred nanometers in mobility diameter are observed. The appearance of these nanometer sized particles corresponds to an increase in organic gas emission in regime 2 (Figs. 1A and 1C). This suggests nucleation is occurring that involves higher molecular mass/lower volatility organics, perhaps with inorganic seeds such as sulfuric acid[65] that are known to initiate new particle formation in ambient air. The resulting nucleated ultrafine particles appeared in general at critical temperatures ranging from 147°C – 277°C for each brake type which is in line with a previous reported range of 140-240°C.[39,57,58] The only exception was the experiment performed with a fresh ceramic brake (exp #77) which had much higher VOC emissions, and hence the nucleation event happened at a lower temperature (T = 128°C). Nucleation from vapors emitted from the brake pads was also observed during a separate heating-only experiment where a piece of commercial brake pad was heated step-wise up to 250°C in a closed cell (data not shown). This supports the hypothesis that gaseous organics emitted during braking are responsible for forming new particles in regime 2. The detailed processes governing these processes are the subject of current studies.

Volatile organic compounds distribution. A total of 85 individual VOC was identified and quantified in the WAS samples, with an additional ~ 20 compounds tentatively identified for which standards were not available. One striking observation is the relatively high amount of CO measured from brakes (orders of magnitude above background, Fig. 1) but surprisingly little carbon dioxide (CO_2, only double the background, Fig. S7). This ratio of CO/CO_2 is often associated with a low-combustion efficiency processes such as smoldering fires and was the case for both regimes 1 and 2. Figure 2 shows the overall emission ratio (ER; $\Delta VOC/\Delta CO$) distribution of the VOC measured in regime 2 classified by chemical groups. Quantitative ER values and standard deviations for each individual VOC for both types of brakes are given in Table S4 and S5 respectively. Common components include alkanes, alkenes, alkynes and aromatics compounds as well as alcohols, and carbonyls, with a notable contribution from nitriles. Note that a significant amount of methane was observed in both brake type experiments, with ER values of 81 and 76 pptv/ppbv CO for the ceramic and semi-metallic brakes respectively (Fig. S8; Table S1). Methane emission ratios observed in this study for brakes are the same order of magnitude as that from biomass burning (Fig. 3D). This potentially has important climate implications, as methane is an important greenhouse gas.

The nature of the individual VOC is similar for both types of brake pads, but there is some variation in the relative contributions of different classes of compounds. For example, the semi-metallic brakes emit more alkanes and less aromatic compounds (Fig. 2). Figure 3A presents the average emissions of the 25 most abundant VOC measured in regime 2 as a ratio to CO for the six experiments performed with ceramic brake pads; similar ER data for the semi-metallic brakes are shown in Fig. 3B, with a direct comparison between the two brakes in Fig. 3C. It is noteworthy that a similar set of VOC have been identified from combustion of 18 different biomass fuels characteristic of three different regions of the U.S. (north, southeast, southwest) under controlled laboratory conditions[59] as well as in wildfire plumes (Figs. 3D and S9A). More than half of the top 25 compounds from both brakes are also in the top 25 from biomass burning. In addition, smaller contributors to the total VOC pool included furans and halogenated compounds (dominated by CH_3Cl), that are characteristic of biomass burning plumes,[59-62] and whose emissions are commonly not found in typical urban settings. Note that biomass burning

emissions vary by fuel and conditions such as temperature and stage of the fire,[60,61,63] and a 1-to-1 correlation with biomass burning is not expected; it is nonetheless intriguing that brake emissions share such similarities with biomass burning plumes (Fig. 3D).

Significant amounts of NO_x are generated during heavy braking (Figs. 1 and S6) along with VOC, and their reactions in air generate ozone (O_3) and other oxidants, as well as particles.[41] Both O_3 and particles have climate and health impacts.[22] Since a major loss process for VOC in the atmosphere that initiates this chemistry is reaction with the hydroxyl (OH) radical, the relative contributions to reactivity for individual VOC compared to that of CO can be estimated by $k_{OH}\times[VOC_i] / k'_{OH}\times[CO]$, where k_{OH} is the second-order rate constant for the reaction of the individual organic (VOC_i) with OH (Table S6) and k'_{OH} is the second-order rate constant for OH with CO (2.4×10^{-13} cm^3 $molecule^{-1}$ s^{-1}). Comparing the relative reactivities of brake emissions, illustrated in Figs. 4A and 4B (with a direct comparison in Fig. 4C), with those reported for biomass burning (Figs. 4D and S9B),[59] it is evident that a significant overlap exists between the most reactive compounds for brake and biomass burning emissions, with alkenes and carbonyls being major contributors in both cases. Note that the total reactivity relative to CO in Figs. 4A and 4B is somewhat higher for the brakes compared to that of biomass burning (Fig. 4D).

Real-time analysis of the emitted gases was also carried out using PTR-MS which detects and measures some species that were not possible to measure by WAS. It also provides elemental composition for individual compounds that are sufficiently volatile to remain in the gas phase. Figure S10 shows typical unit-resolution mass spectra for the two types of brake pads measured during regime 2, and the exact masses and elemental formulae from the high-resolution mass spectra are summarized in Table S7. A total of 93 individual ions were identified, with most having also been previously identified in biomass burning plumes also by PTR-MS.[61,63-68] Of specific interest is the detection of formaldehyde, phenol, hydrogen cyanide (HCN) and isocyanic acid (HNCO) and a variety of nitrogen-containing organics including pyrrole, pyridine and a series of nitriles. Emission ratios for these VOC were estimated using the integrated VOC concentrations measured by the PTR-MS at the same time as WAS canisters were collected. These VOC were ratioed to CO concentrations determined by WAS and averaged across the six experiments performed for each brake pad type. Note that VOCs associated with brake fluid

vapors, which are glycol ethers (Table S7), were often observed at the highest temperatures, but typically not in large quantity for these experiments. Results are presented in Fig. 5 (stippled bars for ceramic brakes; solid colors for semi-metallic brakes), grouped by functional classes. Ammonia (NH_3), known to be present in car exhaust,[69] was also a significant contributor. A noticeable difference between the two types of brakes is the relatively larger concentrations and numbers of nitrogen-containing compounds for the ceramic brake compared to the semi-metallic brake pad emissions, likely linked to the differences in their proprietary formulations.

Our measurements (Figs. S11A and S11B) also show small concentrations of ethylbenzene and xylenes compared to that of benzene for both brake types, in good agreement with Placha et al.[40] It is evident from Fig. S11 that the ER values of ethylbenzene and xylenes are much smaller in brakes compared to tailpipe emissions (Fig. S11C). Thus, these ratios may serve to differentiate brake from tailpipe emissions in air. Notably, the ratios for BTEX from brakes, as well as acetonitrile, match fairly well those of biomass burning samples from both laboratory burns and wildfires (Fig. S11D).

Nitrogen compounds detected from brakes (Fig. 5) have also been reported in biomass burning plumes.[64,66,70,71] Some components such as nitrogen-containing organics and phenol will react in air to form light-absorbing aerosol particles known as brown carbon,[72] also potentially impacting climate. Nitriles, especially acetonitrile, have been suggested as markers for biomass burning,[59,64] and the higher concentrations from brakes may also make them useful for tracking brake emissions.

Brake pads contain a complex mixture of organic and inorganic components, with phenolic resins as a common and significant constituent.[48,73,74] The synthesis of these resins often involves diisocyanates and a tertiary amine, incorporating nitrogen and cyano groups into the brake pads.[43,45,75] Additives such as silicone, epoxy- and rubber resins are frequently included.[43,45,73] The synthetic rubbers are often derived from acrylonitrile, and other nitrogen-containing resins based on cyanate esters and aramid pulp, and polybenzoxazines are common components.[45,73,76] Upon decomposition, these materials are expected to release nitriles, such as acetonitrile, acrylonitrile and benzonitrile as major products.[77-79] Lastly, “green” components and natural

fibers derived from plant-based material (e. g. cashew nut shell liquid or cashew dust, cellulose and lignin …etc) have been introduced in the formulation of brake pads.[43-46,80] The strong frictional and thermal forces in the tribological interactions that occur at high brake pad-rotor interface temperatures during braking[81,82] generate a variety of gases that contain carbon, oxygen and nitrogen. The significant contribution of organonitrogen compounds to the gases and particles observed here is consistent with the presence of nitrogenous components in brake pads. It is therefore not surprising that the emissions from degradation of the organic components in the brake pads have similarities to those of biomass burning.

Furthermore, studies of the thermal decomposition of some phenolic resins report generation of a suite of gases that were also observed here during braking. These include phenol, methane, ethane, ethene, propene, 1-butene, 1-pentene, acetonitrile, propanenitrile, benzonitrile, HCN, NH_3, hydrogen (H_2) and aromatics such as benzene, toluene and the xylenes.[75,83,84] Decomposition of a phenol resin was observed to start around 200°C,[75] similar to regime 2 in the present studies.

Semi-volatile organic compounds. To understand the nature of the observed new particle formation, volatile and semi-volatile organic components (SVOC) with boiling points ranging from 174°C to 356°C (corresponding to C10 (decane) to C21 (heneicosane)) were measured by sampling onto Tenax sorbent cartridges and performing thermal desorption GC-MS analysis. In the SVOC analysis there are more than 300 distinct peaks in the chromatograms, illustrating the complex mixture of gases that are emitted. Figures 6A and 6C summarize the average SVOC organics (C10 and larger) measured for both brake types under the heavy braking conditions of regime 2 grouped by class (variability across experiments is presented in Figs. S13A and S13C). Oxygen and nitrogen-containing organics contribute about 48% of the total SVOC mass for the ceramic brake and 41% for the semi-metallic brake, with hydrocarbons responsible for most of the remainder.

If the SVOC contribute significantly to new particle formation, one might expect some relationship between their distribution and those found in the newly formed particles. Thus, particle composition was also measured simultaneously using a high-resolution time-of-flight

aerosol mass spectrometer (AMS) and is shown grouped by compound class in Fig. 6B for the ceramic brake and Fig. 6D for the semi-metallic brake. These represent averages across three experiments for each brake type with the variation across experiments given in Figs. S13B and S13D. The two types of measurements (SVOC and AMS) show somewhat similar composition for both type of brakes. The largest difference is the nitrogenated species whose contribution is larger in the particles measured by the AMS compared to the SVOC distribution. This could indicate that smaller more volatile species may be trapped in the particles as they grow quickly to > 50-100 nm or may represent species that are not detected by the sorbent tube. These results also align with previous reports of complex mixtures of higher molecular mass organic gases and particles from brakes.[40,85]

Environmental Impacts. There are potential direct impacts of the gas emissions on health and climate. For example, acetonitrile, acetaldehyde, benzene, toluene, the xylenes, methanol, acrolein and phenol are designated as hazardous air pollutants (HAP) by the U.S. Environmental Protection Agency.[86] Given that the brake emissions are at street level, communities in high traffic areas and commuters will continue to be exposed to toxic gases even when the tailpipe emissions have dropped to zero. The major emissions of VOC and SVOC from brake usage are also common to those from biomass burning which have known impacts on health and climate.[6,7,59,87,88] Given the similarity to biomass burning and the potential increasing usage of eco-friendly natural fibers, fillers and binders in brake manufacturing, emissions from "ZEEV" vehicles might be described as due to a *slow-burning, continuous wildfire,* that would persist even when tailpipe emissions are eliminated. Although brake emissions from individual brake pads may not be as large on an absolute scale as those from individual wildfires, brake emissions are not episodic, but are ongoing and cumulative in urban areas.

Some of the gases associated with brake emissions, such as directly emitted methane and ozone formed from secondary VOC-NO_x reactions, are greenhouse gases. Others such as H_2 measured in the present studies (Fig. S12) and reported by others[61,89] have an indirect effect by reacting with OH radicals in air, reducing the OH concentration and hence increasing the lifetimes of other species with which it reacts such as methane.[90] The H_2 emissions measured in these studies

are sufficiently small that they are unlikely to be important compared to other sources,[61,89] for example, leakage from pipelines and storage facilities. However, as the use of H_2 as a replacement fuel increases, emissions associated with brakes should be included in the hydrogen budget.

Quantifying the contribution of brake emissions to air quality is challenging due to the lack of unique markers. In a number of studies,[13,15,16,24,26,34,91,92] source apportionment techniques have been applied using different combinations of trace metals in particles to estimate the contribution of brakes to airborne particulate matter. While this approach is useful, it is complicated by the number of different sources of airborne metals, and in addition, some markers used for brake pads such as copper are being phased out. In terms of potential gas phase markers, acetonitrile has been suggested as a marker for biomass burning,[59,64] and the higher concentrations from brakes compared to exhaust also support its use as a marker of brake emissions in the absence of wildfires. Thus, the ratio of acetonitrile to CO in biomass burning plumes has been reported as 2.01 ± 0.16 pptv/ppbv, an order of magnitude larger than in urban air, 0.26 ±0.16 pptv/ppbv.[93] In the present studies, this ratio was 1.8 ± 1.3 pptv/ppbv CO for ceramic brakes and 5.6 ± 1.7 pptv/ppbv CO for semi-metallic brakes in regime 1. In regime 2, the ratio was 15.7 ± 3.9 pptv/ppbv CO and 7.7 ± 1.0 pptv/ppbv CO for ceramic and semi-metallic brakes respectively (Table S4 and S5). Other nitriles which are emitted at lower levels such as propanenitrile, acrylonitrile and benzonitrile may also make them useful for estimating brake emissions. Nitriles are relatively slow to react in air (Table S6) and lifetimes with respect to OH radicals are estimated to be on the order of 3 to 526 days at typical OH radical concentration of 10^6 cm^{-3}.

Another potential marker of brake emissions is phenol.[40] The phenol-to-CO ratio from brakes measured using PTR-MS for phenol is as high as 17 pptv/ppbv CO for the semi-metallic brake (regime 2; the value for the ceramic brakes was 3.6 pptv/ppbv CO), significantly larger than that reported from biomass burning, 0.5-2.1 pptv/ppbv CO.[59] With much lower temperatures recorded in regime 1, the phenol-to-CO ratio was 0.12 pptv/ppbv CO for the semi-metallic brake (there was no correlation with CO for the ceramic brake). The rate constant for OH reaction with phenol is 2.7×10^{-11} cm^3 $molecule^{-1}$ s^{-1} at 296 K.[94,95] Using an average OH radical

concentration of 10^6 cm^{-3}, the lifetime of phenol with respect to OH corresponds to approximately 10 hours.

With continuous brake emissions that may be found near heavily trafficked roads and the low reactivity with OH, phenol and nitriles may be detectable. For example, previous studies[96,97] reported acetonitrile near roadsides and attributed its source to traffic, however acetonitrile is low in tailpipe measurements of common light duty vehicles.[98,99] Our findings suggest that emissions from brakes may have contributed to their observations. The key attribute of such markers is that they are not found in significant concentrations from modern tailpipe emissions.[100] Sampling of the exhaust of several passenger vehicle showed that phenol was present only at very low concentrations (Fig. S11C). Thus acetonitrile and phenol may be good markers for brake emissions, and BTEX ratios for tailpipe emissions (Figs. S11A and S11B) to provide useful source apportionment capabilities in heavily trafficked urban settings going forward. Future studies are needed to confirm unique markers for brake emissions and to measure them in urban environments so that their impacts on air quality and climate can be quantified.

While technology such as electrostatic precipitators have been in development to remove particulate matter emitted from brakes, no solution has yet been proposed to reduce emissions of gases. Elucidation and speciation of the VOC emitted will allow mitigation strategies to be developed and implemented. This could include, for example, solid sorbent traps that capture the VOC before their release into the atmosphere, and/or designing heat-resistant brake pad materials[81] that will produce fewer toxic VOC.

Acknowledgements:

Funding: We are grateful to the California Department of Justice and the National Science Foundation (grant # 2327825) for support of this work. We also thank M. Steinborn and S. Embleton for assistance with the dynamometer, Professors J. Bullock, B. Boden-Albala and P. Khargonekar for their support. The authors acknowledge the use of facilities and instrumentation at the UC Irvine Materials Research Institute (IMRI), which is supported in part by the National Science Foundation through the UC Irvine Materials Research Science and Engineering Center (DMR-2011967).

Figure Captions:

Figure 1. Time profile of gas phase species and particles recorded during a typical brake dynamometer experiment using the ceramic brake pad (A-B) and the semi-metallic brake pad (C-D). Panels A and C show the time profiles of gas phase species including total equivalent VOC mixing ratio measured by PTR-MS (green trace; 1 min average; the dark green symbols highlight when the WAS canisters were collected), NO (red trace) and NO_2 (blue trace) mixing ratios measured using a chemiluminescence analyzer, CO (yellow trace) mixing ratio measured using a CO monitor as well as measured in the WAS canisters (dark yellow triangles). The rotor temperature measured during the experiment is indicated by the grey trace. Panels (B and D) show the particle size distributions measured using a scanning mobility particle sizer (SMPS) and aerodynamic particle sizer (APS). Rotation of the rotor occurred without braking for several minutes before the first braking regime was applied ('*spinning only*' condition). Regime 1 corresponds to light braking conditions while regime 2 corresponds to heavy braking conditions. The rapid decrease of VOC and other trace gases at the end of the experiment is observed as soon as braking stops, which is associated with a cooling of the rotor temperature and dilution as the chamber is continuously flushed with air.

Figure 2. Volatile organic compound distribution. Distribution of emission ratios (relative to CO) from VOC measured simultaneously using whole air sampling (WAS) collected in regime 2 for (A) ceramic brakes and (B) semi-metallic brakes, averaged over six brake dynamometer experiments per brake type. Note that the alkane category does not include CH_4. Additionally, the C1-C2 halogens category, dominated by CH_3Cl, was omitted because its contribution was less than 0.2% for both brake types. Labels include MTs for monoterpenes and S-cpds for sulfur-containing compounds. Table S1 and Fig. S8 provide information on the experimental variability across experiments

Figure 3. Average emission ratios of individual VOC (top 25) relative to CO. Average emission ratios from (A) ceramic brakes and (B) semi-metallic brakes measured using whole air sampling (WAS) collected in regime 2, averaged over six brake dynamometer experiments per brake type and ranked from the most abundant to the least. Error bars for emission ratios represent one standard deviation and are used to determine the corresponding error in relative reactivity. Panel C is a direct comparison between the two brake types. Biomass burning data in panel D were taken from Gilman et al. (2015) and represent laboratory biomass burning studies for combustion of some fuels characteristic of the north (N), southeast (SE) and southwest (SW) regions of the United States.[59] In all panels, TMB stands for trimethylbenzene.

Figure 4. Relative reactivity of individual VOC compounds (top 25) compared to that of CO. Relative reactivity of individual VOC from (A) ceramic brakes and (B) semi-metallic brakes based on emission ratios determined in Fig. 3. Errors bars represent 1 standard deviation calculated from the error in the ER values from Fig. 3, without taking into account the error in the rate constants. Panel C is a direct comparison between the two brake types. TMB stands for trimethylbenzene. For each brake, the total reactivity was calculated similarly to ref. 59 using

$total\ OH\ reactivity = \sum(ER \times k_{OH} \times 2.46 \times 10^{10}\ \text{molecules cm}^{-3}\ \text{ppbv}^{-1})$ taking into account the top 25 VOCs listed.

Figure 5. Average emission ratios (ER) of VOC measured with the PTR-MS grouped by functional and structural group class for the ceramic brake (stippled bars) and the semi-metallic brake (solid colored bars). These ER were determined during regime 2 conditions and averaged over six dynamometer experiments per brake type. The C_xH_y category corresponds exclusively to unsubstituted compounds, and substituted VOC with multiple functional groups were counted once in each appropriate functional group category. The contributions from several important VOC with high ER are indicated in separate colors, while the rest of the compounds of a given family are represented in red. NH_3 almost systematically saturated the instrument during regime 2, even with the dilution on, and was excluded from this plot. The contribution from specific brake fluid VOCs (i. e. glycol ethers, see Table S7) was small during these experiments, and to keep the focus strictly on brake emission, these were not included here. Note that some contribution of brake fluid to *m/z* 45 ($C_2H_7O^+$) cannot be excluded.

Figure 6. Average semi-volatile organic compound ($\geq C_{10}$) distribution and particle chemical composition measured simultaneously for ceramic or semi-metallic brake pads under heavy braking conditions (regime 2). Mass distributions of (A) SVOC with 10 carbons and more and, (B) particle components for ceramic brakes. Mass distributions of (C) SVOC with 10 carbons and more and (D) particle components for semi-metallic brakes. The SVOC analyses represent an average of 6 experiments per brake type, while the particle analyses represent an average of 3 experiments. No sulfur-containing compounds identified in the SVOCs category, while in panels (B) and (D), sulfur compounds include $C_xH_yS_z^+$ as well as $HS_xO_y^+$ fragments. No halocarbons were identified in the SVOCs category. Figure S13 shows data for each experiment and the corresponding average.

References

1. E. von Schneidemesser, P. S. Monks, J. D. Allan, L. Bruhwiler, P. Forster, D. Fowler, A. Lauer, W. T. Morgan, P. Paasonen, M. Righi, K. Sindelarova, M. A. Sutton, Chemistry and the linkages between air quality and climate change, *Chem. Rev.,* 2015, **115**, 3856-3897.
2. M. Saunois, A. R. Stavert, B. Poulter, P. Bousquet, J. G. Canadell, R. B. Jackson, P. A. Raymond, E. J. Dlugokencky, S. Houweling, P. K. Patra, P. Ciais, V. K. Arora, D. Bastviken, P. Bergamaschi, D. R. Blake, G. Brailsford, L. Bruhwiler, K. M. Carlson, M. Carrol, S. Castaldi, N. Chandra, C. Crevoisier, P. M. Crill, K. Covey, C. L. Curry, G. Etiope, C. Frankenberg, N. Gedney, M. I. Hegglin, L. Hoglund-Isaksson, G. Hugelius, M. Ishizawa, A. Ito, G. Janssens-Maenhout, K. M. Jensen, F. Joos, T. Kleinen, P. B. Krummel, R. L. Langenfelds, G. G. Laruelle, L. C. Liu, T. Machida, S. Maksyutov, K. C. McDonald, J. McNorton, P. A. Miller, J. R. Melton, I. Morino, J. Muller, F. Murguia-Flores, V. Naik, Y. Niwa, S. Noce, S. O. Doherty, R. J. Parker, C. H. Peng, S. S. Peng, G. P. Peters, C. Prigent, R. Prinn, M. Ramonet, P. Regnier, W. J. Riley, J. A. Rosentreter, A. Segers, I. J. Simpson, H. Shi, S. J. Smith, L. P. Steele, B. F. Thornton, H. Q. Tian, Y. Tohjima, F. N. Tubiello, A. Tsuruta, N. Viovy, A. Voulgarakis, T. S. Weber, M. van Weele, G. R. van der Werf, R. F. Weiss, D. Worthy, D. Wunch, Y. Yin, Y. Yoshida, W. X. Zhang, Z. Zhang, Y. H. Zhao, B. Zheng, Q. Zhu, Q. A. Zhu, Q. L. Zhuang, The global methane budget 2000-2017, *Earth Sys. Sci. Data,* 2020, **12**, 1561-1623.
3. V. Masson-Delmotte, P. Zhai, A. Pirani, S. L. Connors, C. Péan, S. Berger, N. Caud, Y. Chen, L. Goldfarb, M. Gomis, M. Huang, K. Leitzell, E. Lonnoy, L. B. R. Matthews, T. K. Maycock, T. Waterfield, O. Yelekçi, R. Yu, B. Zhou (2021) IPCC, 2021: Climate Change 2021: The Physical Science Basis. Contribution of Working Group I to the Sixth Assessment Report of the Intergovernmental Panel on Climate Change. (United Kingdom and New York).
4. M. W. Jones, J. T. Abatzoglou, S. Veraverbeke, N. Andela, G. Lasslop, M. Forkel, A. J. P. Smith, C. Burton, R. A. Betts, G. R. van der Werf, S. Sitch, J. G. Canadell, C. Santin, C. Kolden, S. H. Doerr, C. Le Quere, Global and regional trends and drivers of fire under climate change, *Rev. Geophys.,* 2022, **60**, e2020RG000726.
5. X. X. Liu, L. G. Huey, R. J. Yokelson, V. Selimovic, I. J. Simpson, M. Muller, J. L. Jimenez, P. Campuzano-Jost, A. J. Beyersdorf, D. R. Blake, Z. Butterfield, Y. Choi, J. D. Crounse, D. A. Day, G. S. Diskin, M. K. Dubey, E. Fortner, T. F. Hanisco, W. W. Hu, L. E. King, L. Kleinman, S. Meinardi, T. Mikoviny, T. B. Onasch, B. B. Palm, J. Peischl, I. B. Pollack, T. B. Ryerson, G. W. Sachse, A. J. Sedlacek, J. E. Shilling, S. Springston, J. M. St Clair, D. J. Tanner, A. P. Teng, P. O. Wennberg, A. Wisthaler, G. M. Wolfe, Airborne measurements of western US wildfire emissions: Comparison with prescribed burning and air quality implications, *J. Geophys. Res.,* 2017, **122**, 6108-6129.
6. A. Karanasiou, A. Alastuey, F. Amato, M. Renzi, M. Stafoggia, A. Tobias, C. Reche, F. Forastiere, S. Gumy, P. Mudu, X. Querol, Short-term health effects from outdoor exposure to biomass burning emissions: a review, *Sci. Total Environ.,* 2021, **781**, Art. No 146739.
7. M. Keywood, M. Kanakidou, A. Stohl, F. Dentener, G. Grassi, C. P. Meyer, K. Torseth, D. Edwards, A. M. Thompson, U. Lohmann, J. Burrows, Fire in the air: biomass burning impacts in a changing climate, *Crit. Rev. Env. Sci. Technol.,* 2013, **43**, 40-83.

8. G. A. Bishop, Three decades of on-road mobile source emissions reductions in South Los Angeles, *J. Air Waste Manage. Assoc.,* 2019, **69**, 967-976.
9. G. T. Drozd, Y. L. Zhao, G. Saliba, B. Frodin, C. Maddox, R. J. Weber, M. C. O. Chang, H. Maldonado, S. Sardar, A. L. Robinson, A. H. Goldstein, Time resolved measurements of speciated tailpipe emissions from motor vehicles: trends with emission control technology, cold start effects, and speciation, *Environ. Sci. Technol.,* 2016, **50**, 13592-13599.
10. T. V. Johnson, Review of vehicular emissions trends, *SAE Int. J. Engines,* 2015, **8**, 1152-1167.
11. Y. B. Pang, M. Fuentes, P. Rieger, Trends in selected ambient volatile organic compound (VOC) concentrations and a comparison to mobile source emission trends in California's South Coast Air Basin, *Atmos. Environ.,* 2015, **122**, 686-695.
12. S. L. Winkler, J. E. Anderson, L. Garza, W. C. Ruona, R. Vogt, T. J. Wallington, Vehicle criteria pollutant (PM, NO_x, CO, HCs) emissions: How low should we go?, *Npj Climate Atmos. Sci.,* 2018, **1**, Art. No 26.
13. A. Piscitello, C. Bianco, A. Casasso, R. Sethi, Non-exhaust traffic emissions: Sources, characterization, and mitigation measures, *Sci. Total Environ.,* 2021, **766**, Art. No 144440.
14. J. Kukutschova, P. Filip, "Review of brake wear emissions: Identification of gaps and future needs" in Non-exhaust emissions. An urban air quality problem for public health; impact and mitigation measures, F. Amato, Ed. (Academic Press, 2018), 10.1016/B978-0-12-811770-5.00006-6, pp. 123-146.
15. J. C. Fussell, M. Franklin, D. C. Green, M. Gustafsson, R. M. Harrison, W. Hicks, F. J. Kelly, F. Kishta, M. R. Miller, I. S. Mudway, F. Oroumiyeh, L. Selley, M. Wang, Y. F. Zhu, A review of road traffic-derived non-exhaust particles: Emissions, physicochemical characteristics, health risks, and mitigation measures, *Environ. Sci. Technol.,* 2022, **56**, 6813-6835.
16. R. M. Harrison, J. Allan, D. Carruthers, M. R. Heal, A. C. Lewis, B. Marner, T. Murrells, a. Williams, Non-exhaust vehicle emissions of particulate matter and VOC from road traffic: A review, *Atmos. Env.,* 2021, **262**, Art. No 118592.
17. M. L. Kreider, J. M. Panko, B. L. McAtee, L. I. Sweet, B. L. Finley, Physical and chemical characterization of tire-related particles: comparison of particles generated using different methodologies, *Sci. Total Environ.,* 2010, **408**, 652-659.
18. Z. Y. Men, X. F. Zhang, J. F. Peng, J. Zhang, T. G. Fang, Q. Y. Guo, N. Wei, Q. J. Zhang, T. Wang, L. Wu, H. J. Mao, Determining factors and parameterization of brake wear particle emission, *J. Hazard. Mater.,* 2022, **434**, Art. No 128856.
19. I. Park, H. Kim, S. Lee, Characteristics of tire wear particles generated in a laboratory simulation of tire/road contact conditions, *J. Aerosol Sci.,* 2018, **124**, 30-40.
20. V. Roubicek, H. Raclavska, D. Juchelkova, P. Filip, Wear and environmental aspects of composite materials for automotive braking industry, *Wear,* 2008, **265**, 167-175.
21. J. Wahlstrom, L. Olander, U. Olofsson, Size, shape, and elemental composition of airborne wear particles from disc brake materials, *Tribol. Lett.,* 2010, **38**, 15-24.
22. P. J. Landrigan, R. Fuller, N. J. R. Acosta, O. Adeyi, R. Arnold, N. Basu, A. B. Balde, R. Bertollini, S. Bose-O'Reilly, J. I. Boufford, P. N. Breysse, T. Chiles, C. Mahidol, A. M. Coll-Seck, M. L. Cropper, J. Fobil, V. Fuster, M. Greenstone, A. Haines, D. Hanrahan, D. Hunter, M. Khare, A. Krupnick, B. Lanphear, B. Lohani, K. Martin, K. V. Mathiasen,

M. A. McTeer, C. J. L. Murray, J. D. Ndahimananjara, F. Perera, J. Potocnik, A. S. Preker, J. Ramesh, J. Rockstrom, C. Salinas, L. D. Samson, K. Sandilya, P. D. Sly, K. R. Smith, A. Steiner, R. B. Stewart, W. A. Suk, O. C. P. van Schayck, G. N. Yadama, K. Yumkella, M. Zhong, The Lancet Commission on pollution and health, *Lancet,* 2018, **391**, 462-512.

23. K. Malachova, J. Kukutschova, Z. Rybkova, H. Sezimova, D. Placha, K. Cabanova, P. Filip, Toxicity and mutagenicity of low-metallic automotive brake pad materials, *Ecotoxicol. Environ. Safety,* 2016, **131**, 37-44.

24. J. Q. Shen, S. Taghvaee, C. La, F. Oroumiyeh, J. Liu, M. Jerrett, S. Weichenthal, I. Del Rosario, M. M. Shafer, B. Ritz, Y. F. Zhu, S. E. Paulson, Aerosol oxidative potential in the greater Los Angeles area: source apportionment and associations with socioeconomic position, *Environ. Sci. Technol.,* 2022, **56**, 17795–17804.

25. Z. Y. Tian, H. Q. Zhao, K. T. Peter, M. Gonzalez, J. Wetzel, C. Wu, X. M. Hu, J. Prat, E. Mudrock, R. Hettinger, A. E. Cortina, R. G. Biswas, F. V. C. Kock, R. Soong, A. Jenne, B. W. Du, F. Hou, H. He, R. Lundeen, A. Gilbreath, R. Sutton, N. L. Scholz, J. W. Davis, M. C. Dodd, A. Simpson, J. K. McIntyre, E. P. Kolodziej, A ubiquitous tire rubber-derived chemical induces acute mortality in coho salmon, *Science,* 2021, **371**, 185-189.

26. J. Liu, S. Banerjee, F. Oroumiyeh, J. Q. Shen, I. del Rosario, J. Lipsitt, S. Paulson, B. Ritz, J. Su, S. Weichenthal, P. Lakey, M. Shiraiwa, Y. F. Zhu, M. Jerrett, Cokriging with a low-cost sensor network to estimate spatial variation of brake and tire-wear metals and oxidative stress potential in Southern California, *Environ. Int.,* 2022, **168**, Art. No 107481.

27. R. Fuller, P. J. Landrigan, K. Balakrishnan, G. Bathan, S. Bose-O'Reilly, M. Brauer, J. Caravanos, T. Chiles, A. Cohen, L. Corra, M. Cropper, G. Ferraro, J. Hanna, D. Hanrahan, H. Hu, D. Hunter, G. Janata, R. Kupka, B. Lanphear, M. Lichtveld, K. Martin, A. Mustapha, E. Sanchez-Triana, K. Sandilya, L. Schaefli, J. Shaw, J. Seddon, W. Suk, M. M. Tellez-Rojo, C. H. Yan, Pollution and health: a progress update, *Lancet Planet. Health,* 2022, **6**, E535-E547.

28. D. W. Dockery, C. A. Pope, X. P. Xu, J. D. Spengler, J. H. Ware, M. E. Fay, B. G. Ferris, F. E. Speizer, An Association between air-pollution and mortality in six United-States cities, *New. Engl. J. Med.,* 1993, **329**, 1753-1759.

29. L. Calderon-Garciduenas, R. Torres-Jardon, M. Franco-Lira, R. Kulesza, A. Gonzalez-Maciel, R. Reynoso-Robles, R. Brito-Aguilar, B. Garcia-Arreola, P. Revueltas-Ficachi, J. A. Barrera-Velazquez, G. Garcia-Alonso, E. Garcia-Rojas, P. S. Mukherjee, R. Delgado-Chavez, Environmental nanoparticles, SARS-CoV-2 brain involvement, and potential acceleration of Alzheimer's and Parkinson's diseases in young urbanites exposed to air pollution, *J. Alzheimers Dis.,* 2020, **78**, 479-503.

30. C. W. Tessum, D. A. Paolella, S. E. Chambliss, J. S. Apte, J. D. Hill, J. D. Marshall, PM2.5 polluters disproportionately and systemically affect people of color in the United States, *Sci. Adv.,* 2021, **7**, eabf4491.

31. A. Jbaily, X. D. Zhou, J. Liu, T. H. Lee, L. Kamareddine, S. Verguet, F. Dominici, Air pollution exposure disparities across US population and income groups, *Nature,* 2022, **601**, 228-233.

32. A. Karanasiou, M. Viana, X. Querol, T. Moreno, F. de Leeuw, Assessment of personal exposure to particulate air pollution during commuting in European cities-Recommendations and policy implications, *Sci. Total Environ.,* 2014, **490**, 785-797.

33. L. D. Knibbs, T. Cole-Hunter, L. Morawska, A review of commuter exposure to ultrafine particles and its health effects, *Atmos. Environ.,* 2011, **45**, 2611-2622.
34. F. Oroumiyeh, M. Jerrett, I. Del Rosario, J. Lipsitt, J. Liu, S. E. Paulson, B. Ritz, J. J. Schauer, M. M. Shafer, J. Q. Shen, S. Weichenthal, S. Banerjee, Y. F. Zhu, Elemental composition of fine and coarse particles across the greater Los Angeles area: Spatial variation and contributing sources, *Environ. Pollut.,* 2022, **292**, Art. No 118356.
35. M. L. Feo, M. Torre, P. Tratzi, F. Battistelli, L. Tomassetti, F. Petracchini, E. Guerriero, V. Paolini, Laboratory and on-road testing for brake wear particle emissions: a review, *Environmental Science and Pollution Research* 2023, **30**, 100282-100300.
36. Y. Liu, S. J. Wu, H. B. Chen, M. Federici, G. Perricone, Y. Li, G. Lv, S. Munir, Z. W. Luo, B. H. Mao, Brake wear induced PM10 emissions during the world harmonised light-duty vehicle test procedure-brake cycle, *J. Cleaner Prod.,* 2022, **361**.
37. M. Mathissen, T. Grigoratos, S. Gramstat, A. Mamakos, R. Vedula, C. Agudelo, J. Grochowicz, B. Giechaskiel, Interlaboratory study on brake particle emissions part II: particle number emissions, *Atmosphere,* 2023, **14**.
38. F. H. F. zum Hagen, M. Mathissen, T. Grabiec, T. Hennicke, M. Rettig, J. Grochowicz, R. Vogt, T. Benter, On-road vehicle measurements of brake wear particle emissions, *Atmos. Environ.,* 2019, **217**.
39. F. H. F. Zum Hagen, M. Mathissen, T. Grabiec, T. Hennicke, M. Rettig, J. Grochowicz, R. Vogt, T. Benter, Study of brake wear particle emissions: impact of braking and cruising conditions, *Environ. Sci. Technol.,* 2019, **53**, 5143-5150.
40. D. Placha, M. Vaculik, M. Mikeska, O. Dutko, P. Peikertova, J. Kukutschova, K. Mamulova Kutlakova, J. Ruzickova, V. Tomasek, P. Filip, Release of volatile organic compounds by oxidative wear of automotive friction materials, *Wear,* 2017, **376**, 705-716.
41. B. J. Finlayson-Pitts, J. N. Pitts, Jr., *Chemistry of the Upper and Lower Atmosphere - Theory, Experiments, and Applications* (Academic Press, San Diego, 2000), pp. 969.
42. A. E. Thomas, P. Bauer, S., M. Dam, V. Perraud, L. M. Wingen, J. Smith, N., Automotive braking is a source of highly charged aerosol particles, *Proc. Natl. Acad. Sci. USA,* 2024, **121**, Art No e2313897121
43. A. Borawski, Conventional and unconventional materials used in the production of brake pads - review, *Sci. Eng. Compos. Mater,* 2020, **27**, 374-396.
44. P. J. Blau (2001) Composition, functions, and testing of friction brake materials and their additivies. (Oak Ridge National Laboratory), pp 1-38.
45. D. Chan, G. W. Stachowiak, Review of automotive brake friction materials, *Proc. Inst. Mech. Eng., Part D,* 2004, **218**, 953-966.
46. A. Thorpe, R. M. Harrison, Sources and properties of non-exhaust particlulate matter from road traffic: a review, *Sci. Total Environ.,* 2008, **400**, 270-282.
47. A. Sinha, G. Ischia, C. Menapace, S. Gialanella, Experimental characterization protocols for wear products from disc brake materials, *Atmosphere,* 2020, **11**.
48. A. Bonfanti (2016) Low-impact friction materials for brake pads. in *Materials Science and Engineering* (University of Trento, Trento, Italy), p 214.
49. M. H. Cho, S. J. Kim, D. Kim, H. Jang, Effects of ingredients on tribological characteristics of a brake lining: an experimental case study, *Wear,* 2005, **258**, 1682-1687.

50. M. H. Cho, S. J. Kim, R. H. Basch, J. W. Fash, H. Jang, Tribological study of gray cast iron with automotive brake linings: The effect of rotor microstructure, *Tribol. Int.,* 2003, **36**, 537-545.
51. T. Grigoratos, C. Agudelo, J. Grochowicz, S. Gramstat, M. Robere, G. Perricone, A. Sin, A. Paulus, M. Zessinger, A. Hortet, S. Ansaloni, R. Vedula, M. Mathissen, Statistical assessment and temperature study from the interlaboratory application of the WLTP-brake cycle, *Atmosphere,* 2020, **11**.
52. A. Stanard, T. DeFries, C. Palacios, S. Kishan (2021) Brake and tire wear emissions, Project 17RD016, Final Report, Rev. 2. (California Air Resources Board), pp 1-158.
53. M. Mathissen, J. Grochowicz, C. Schmidt, R. Vogt, F. H. F. zum Hagen, T. Grabiec, H. Steven, T. Grigoratos, A novel real-world braking cycle for studying brake wear particle emissions, *Wear,* 2018, **414**, 219-226.
54. J. J. Colman, A. L. Swanson, S. Meinardi, B. C. Sive, D. R. Blake, F. S. Rowland, Description of the analysis of a wide range of volatile organic compounds in whole air samples collected during PEM-Tropics A and B, *Anal. Chem.,* 2001, **73**, 3723-3731.
55. J. H. J. Hulskotte, G. D. Roskam, H. van der Gon, Elemental composition of current automotive braking materials and derived air emission factors, *Atmos. Environ.,* 2014, **99**, 436-445.
56. Y. Lv, X. Chen, S. S. Wei, R. Zhu, B. B. Wang, B. Chen, M. Kong, J. S. Zhang, Sources, concentrations, and transport models of ultrafine particles near highways: a literature review, *Build. Environ.,* 2020, **186**, Art. No 107325.
57. H. Niemann, H. Winner, C. Asbach, H. Kaminski, G. Frentz, R. Milczarek, Influence of disc temperature on ultrafine, fine, and coarse particle emissions of passenger car dis brakes with organic and inorganic pad binder materials, *Atmosphere,* 2020, **11**, 1-17.
58. O. Nosko, U. Olofsson, Quantification of ultrafine airborne particulate matter generated by the wear of car brake materials, *Wear,* 2017, **374-375**, 92-96.
59. J. B. Gilman, B. M. Lerner, W. C. Kuster, P. D. Goldan, C. Warneke, P. R. Veres, J. M. Roberts, J. A. de Gouw, I. R. Burling, R. J. Yokelson, Biomass burning emissions and potential air quality impacts of volatile organic compounds and other trace gases from fuels common in the US, *Atmos. Chem. Phys.,* 2015, **15**, 13915-13938.
60. M. O. Andreae, P. Merlet, Emission of trace gases and aerosols from biomass burning, *Global biochemical cycles,* 2001, **15**, 955-966.
61. M. O. Andreae, Emission of trace gases and aerosols from biomass burning - an updated assessment, *Atmos. Chem. Phys.,* 2019, **19**, 8523-8546.
62. R. Koppmann, K. von Czapiewski, J. S. Reid, A review of biomass burning emissions, part I: gaseous emissions of carbon monoxide, methane, volatile organic compounds, and nitrogen containing compounds, *Atmos. Chem. Phys. Discuss.,* 2005, **5**, 10455-10516.
63. K. Sekimoto, A. R. Koss, J. B. Gilman, V. Selimovic, M. M. Coggon, K. J. Zarzana, B. Yuan, B. M. Lerner, S. S. Brown, C. Warneke, R. J. Yokelson, J. M. Roberts, J. de Gouw, High- and low-temperature pyrolysis profiles describe volatile organic compound emissions from western US wildfire fuels, *Atmos. Chem. Phys.,* 2018, **18**, 9263-9281.
64. R. Holzinger, C. Warneke, A. Hansel, A. Jordan, W. Lindinger, D. H. Scharffe, G. Schade, P. J. Crutzen, Biomass burning as a source of formaldehyde, acetaldehyde, methanol, acetone, acetonitrile, and hydrogen cyanide, *Geosphys. Res. Lett.,* 1999, **26**, 1161-1164.

65. T. G. Karl, T. J. Christian, R. J. Yokelson, P. Artaxo, W. M. Hao, A. Guenther, The Tropical Forest and Fire Emissions Experiment: method evaluation of volatile organic compound emissions measured by PTR-MS, FTIR, and GC from tropical biomass burning, *Atmos. Chem. Phys.,* 2007, **7**, 5883-5897.
66. A. R. Koss, K. Sekimoto, J. B. Gilman, V. Selimovic, M. M. Coggon, K. J. Zarzana, B. Yuan, B. M. Lerner, S. S. Brown, J. L. Jimenez, J. Krechmer, J. M. Roberts, C. Warneke, R. J. Yokelson, J. de Gouw, Non-methane organic gas emissions from biomass burning: identification, quantification, and emission factors from PTR-ToF during the FIREX 2016 laboratory experiment, *Atmos. Chem. Phys.,* 2018, **18**, 3299-3319.
67. C. E. Stockwell, P. R. Veres, J. Williams, R. J. Yokelson, Characterization of biomass burning emissions from cooking fires, peat, crop residue, and other fuels with high-resolution proton-transfer-reaction time-of-flight mass spectrometry, *Atmos. Chem. Phys.,* 2015, **15**, 845-865.
68. C. Warneke, J. M. Roberts, P. Veres, J. Gilman, W. C. Kuster, I. Burling, R. Yokelson, J. A. de Gouw, VOC identification and inter-comparison from laboratory biomass burning using PTR-MS and PIT-MS, *Int. J. Mass Spectrom.,* 2011, **303**, 6-14.
69. N. J. Farren, J. Davison, R. A. Rose, R. L. Wagner, D. C. Carslaw, Characterisation of ammonia emissions from gasoline and gasoline hybrid passenger cars, *Atmos Environ-X,* 2021, **11**.
70. R. S. Hornbrook, D. R. Blake, G. S. Diskin, A. Fried, H. E. Fuelberg, S. Meinardi, T. Mikoviny, D. Richter, G. W. Sachse, S. A. Vay, J. Walega, P. Weibring, A. J. Weinheimer, C. Wiedinmyer, A. Wisthaler, A. Hills, D. D. Riemer, E. C. Apel, Observations of nonmethane organic compounds during ARCTAS - Part 1: Biomass burning emissions and plume enhancements, *Atmos. Chem. Phys.,* 2011, **11**, 11103-11130.
71. M. D. Leslie, M. Ridoli, J. G. Murphy, N. Borduas-Dedekind, Isocyanic acid (HNCO) and its fate in the atmosphere: a review, *Environ. Sci. Process, Imp.,* 2019, **21**, 793-808.
72. A. Laskin, J. Laskin, S. A. Nizkorodov, Chemistry of atmospheric brown carbon, *Chem. Rev.,* 2015, **115**, 4335-4382.
73. G. G. di Confiengo, M. G. Faga, Ecological transition in the field of brake pad manufacturing: An overview of the potential green constituents, *Sustainability,* 2022, **14**, Art. No 2508.
74. A. Borawski, Testing passenger car brake pad exploitation time's impact on the values of the coefficient of friction and abrasive wear rate using a pin-on-disc method, *Materials,* 2022, **15**, Art. No 1991.
75. C. A. Lytle, W. Bertsch, M. D. McKinley, Determination of thermal decomposition products from a phenolic urethane resin by pyrolysis gas chromatography mass spectrometry, *J. High Res. Chrom.,* 1998, **21**, 128-132.
76. W. Lertwassana, T. Parnklang, P. Mora, C. Jubsilp, S. Rimdusit, High performance aramid pulp/carbon fiber-reinforced polybenzoxazine composites as friction materials, *Compos. Part B-Eng.,* 2019, **177**.
77. J. R. Brown, A. J. Power, Thermal-Degradation of Aramids .2. Pyrolysis-Gas Chromatography-Mass Spectrometry of Some Model Compounds of Poly(1,3-Phenylene Isophthalamide) and Poly(1,4-Phenylene Terephthalamide), *Polym. Degrad. Stab.,* 1982, **4**, 479-490.

78. G. M. Cai, W. D. Yu, Study on the thermal degradation of high performance fibers by TG/FTIR and Py-GC/MS, *J. Therm. Anal. Calorim.,* 2011, **104**, 757-763.
79. P. Perlstein, Identification of Fibers and Fiber Blends by Pyrolysis-Gas Chromatography, *Anal. Chim. Acta,* 1983, **155**, 173-181.
80. P. Filip, L. Kovarik, M. A. Wright, Automotive brake lining characterization, *SAE International,* 1997, https://doi.org/10.4271/973024, Art No 973024.
81. B. S. Joo, Y. H. Chang, H. J. Seo, H. Jang, Effects of binder resin on tribological properties and particle emission of brake linings, *Wear,* 2019, **434**.
82. T. E. Fischer, Tribochemistry, *Ann. Rev. Mater. Sci.,* 1988, **18**, 302-323.
83. A. Bennett, D. R. Payne, R. W. Court, Pyrolytic and elemental analysis of decomposition products from a phenolic resin, *Macromolecular Symposia,* 2014, **339**, 38-47.
84. F. Torres-Herrador, A. Eschenbacher, J. Coheur, J. Blondeau, T. E. Magin, K. M. Van Geem, Decomposition of carbon/phenolic composites for aerospace heatshields: Detailed speciation of phenolic resin pyrolysis products, *Aerosp. Sci. Technol.,* 2021, **119**, Art. No 107079.
85. C. Alves, M. Evtyugina, A. Vicente, E. Conca, F. Amato, Organic profiles of brake wear particles, *Atmos. Res.,* 2021, **255**, Art. No 105557.
86. U.S. Environmental Protection Agency (2023) Hazardous Air Pollutants. (United States Environmental Protection Agency).
87. J. M. Chen, C. L. Li, Z. Ristovski, A. Milic, Y. T. Gu, M. S. Islam, S. X. Wang, J. M. Hao, H. F. Zhang, C. R. He, H. Guo, H. B. Fu, B. Miljevic, L. Morawska, P. Thai, Y. F. Lam, G. Pereira, A. J. Ding, X. Huang, U. C. Dumka, A review of biomass burning: Emissions and impacts on air quality, health and climate in China, *Sci. Total Environ.,* 2017, **579**, 1000-1034.
88. Y. W. Li, Cloud condensation nuclei activity and hygroscopicity of fresh and aged biomass burning particles, *Pure Appl. Geophys.,* 2019, **176**, 345-356.
89. G. Pieterse, M. C. Krol, A. M. Batenburg, L. P. Steele, P. B. Krummel, R. L. Langenfelds, T. Rockmann, Global modelling of H_2 mixing ratios and isotopic compositions with the TM5 model, *Atmos. Chem. Phys.,* 2011, **11**, 7001-7026.
90. I. B. Ocko, S. P. Hamburg, Climate consequences of hydrogen emissions, *Atmos. Chem. Phys.,* 2022, **22**, 9349-9368.
91. X. Wang, S. Gronstal, B. Lopez, H. Jung, L.-W. A. Chen, G. Wu, S. S. H. Ho, J. C. Chow, J. G. Waston, Q. Yao, S. Yoon, Evidence of non-tailpipe emission contributions to PM2.5 and PM10 near southern California highways, *Environ. Pollut.,* 2023, **317**, Art. No 120691.
92. M. M. Badami, R. Tohidi, V. J. Farahani, C. Sioutas, Size-segregated source identification of water-soluble and water-insoluble metals and trace elements of coarse and fine PM in central Los Angeles, *Atmos. Environ.,* 2023, **310**, Art. No119984.
93. Y. Huangfu, B. Yuan, S. H. Wang, C. H. Wu, X. J. He, J. P. Qi, J. de Gouw, C. Warneke, J. B. Gilman, A. Wisthaler, T. Karl, M. Graus, B. T. Jobson, M. Shao, Revisiting acetonitrile as tracer of biomass burning in anthropogenic-influenced environments, *Geosphys. Res. Lett.,* 2021, **48**.
94. M. Rinke, C. Zetzsch, Rate constants for the reaction of OH radicals with aromatics: benzene, phenol, aniline, and 1,2,4-trichlorobenzene, *Ber. Bunsen-Ges. Phys. Chem,* 1984, **88**, 55-62.

95. M. Semadeni, D. W. Stocker, J. A. Kerr, The temperature dependence of the OH radical reactions with some aromatic compounds under simulated tropospheric conditions, *Int. J. Chem. Kinet.,* 1995, **27**, 287-304.

96. R. Holzinger, A. Jordan, A. Hansel, W. Lindinger, Automobile emissions of acetonitrile: assessment of its contribution to the global source, *J. Atmos. Chem.,* 2001, **38**, 187-193.

97. A. C. Valach, B. Langford, E. Nemitz, A. R. MacKensie, C. N. Hewitt, Concentrations of selected volatile organic compounds at kerbside andbackground sites in central London, *Atmos. Environ.,* 2014, **95**, 456-467.

98. A. H. Goldstein, A. Robinson, J. Kroll, G. T. Drozd, Y. H. Zhao, G. Saliba, S. R., A. Presto (2017) Investigating semi-volatile organic compound emissions from light-duty vehicles. (California Air Resources Board Report,), pp 1-225.

99. B. Marques, E. Kostenidou, A. M. Valiente, B. Vansevenant, T. Sarica, L. Fine, B. Temime-Roussel, P. Tassel, P. Perret, Y. Liu, K. Sartelet, C. Ferronato, B. D'Anna, Detailed speciation of non-methane volatile organic compounds in exhaust emissions from diesel and gasoline Euro 5 vehicles using online and offline measurements, *Toxics,* 2022, **10**, Art No 184, doi: 110.3390/toxics10040184.

100. M. G. Perrone, C. Carbone, D. Faedo, L. Ferrero, A. Maggioni, G. Sangiorgi, E. Bolzacchini, Exhaust emissions of polycyclic aromatic hydrocarbons, n-alkanes and phenols from vehicles coming within different European classes, *Atmos. Environ.,* 2014, **82**, 391-400.

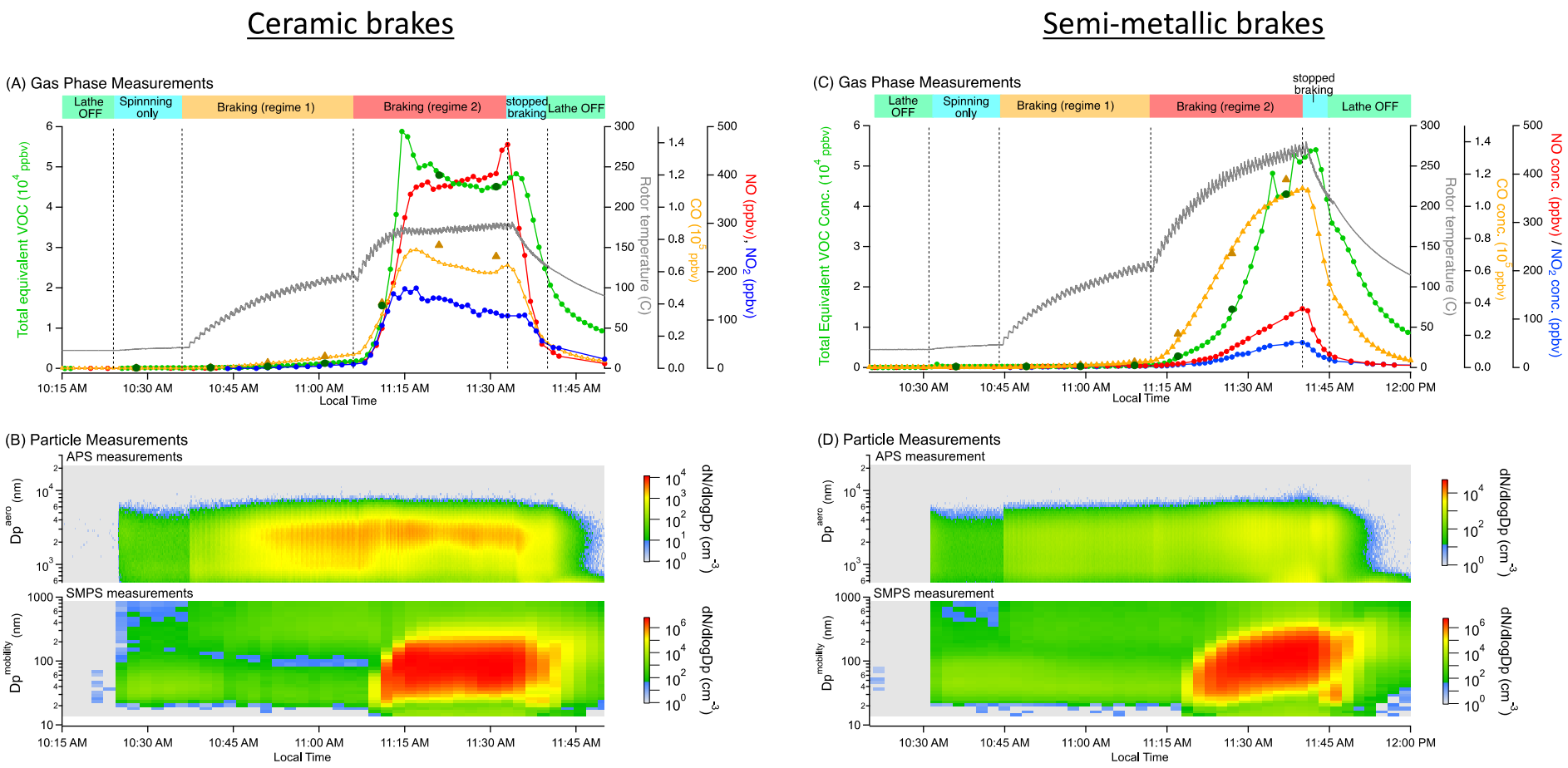

Figure 1. Time profile of gas phase species and particles recorded during a typical brake dynamometer experiment using the ceramic brake pad (A-B) and the semi-metallic brake pad (C-D). Panels A and C show the time profiles of gas phase species including total equivalent VOC mixing ratio measured by PTR-MS (green trace; 1 min average; the dark green symbols highlight when the WAS canisters were collected), NO (red trace) and NO_2 (blue trace) mixing ratios measured using a chemiluminescence analyzer, CO (yellow trace) mixing ratio measured using a CO monitor as well as measured in the WAS canisters (dark yellow triangles). The rotor temperature measured during the experiment is indicated by the grey trace. Panels (B and D) show the particle size distributions measured using a scanning mobility particle sizer (SMPS) and aerodynamic particle sizer (APS). Rotation of the

rotor occurred without braking for several minutes before the first braking regime was applied ('*spinning only*' condition). Regime 1 corresponds to light braking conditions while regime 2 corresponds to heavy braking conditions. The rapid decrease of VOC and other trace gases at the end of the experiment is observed as soon as braking stops, which is associated with a cooling of the rotor temperature and dilution as the chamber is continuously flushed with air.

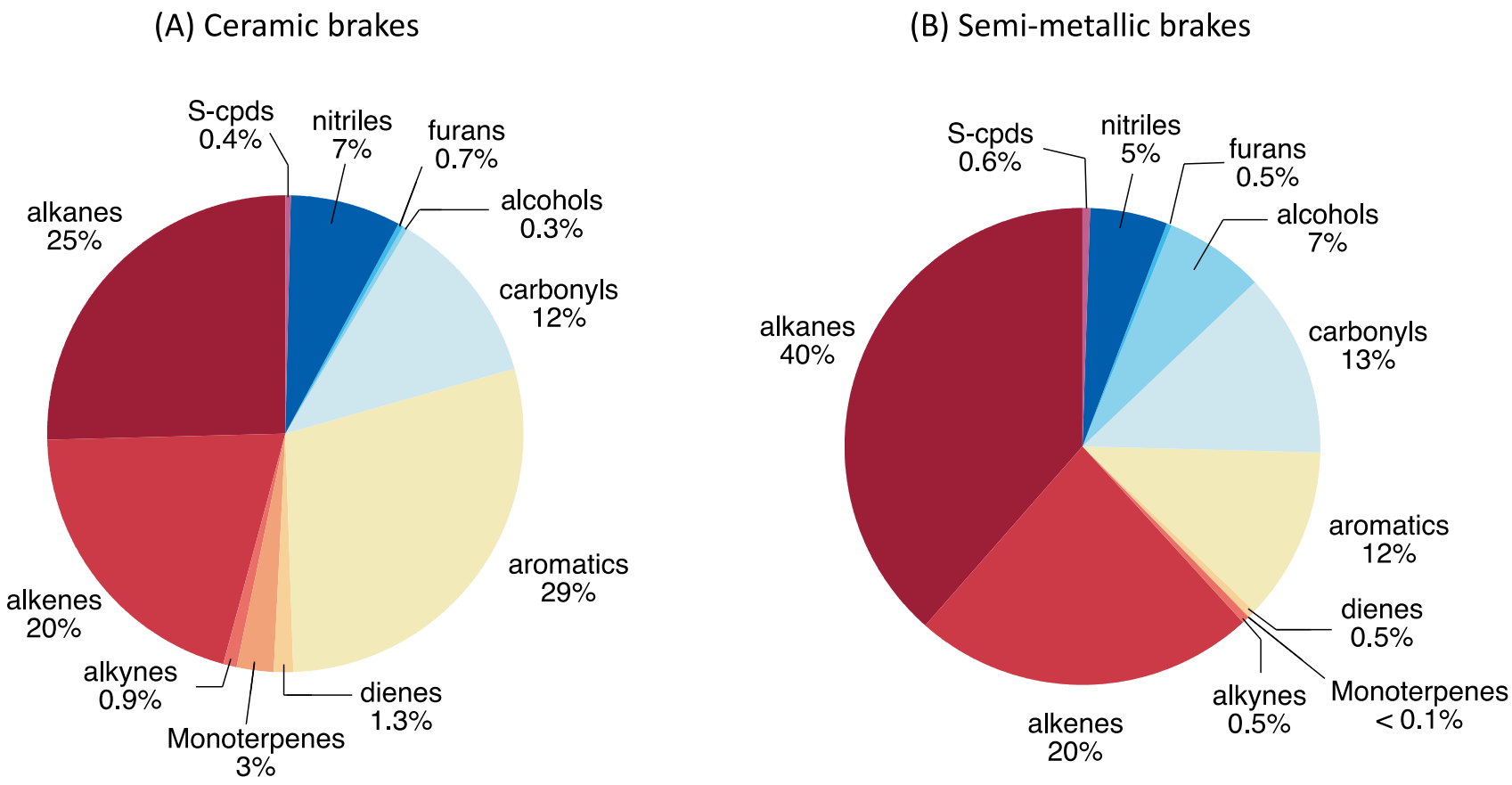

Figure 2. Volatile organic compound distribution. Distribution of emission ratios (relative to CO) from VOC measured simultaneously using whole air sampling (WAS) collected in regime 2 for (A) ceramic brakes and (B) semi-metallic brakes, averaged over six brake dynamometer experiments per brake type. Note that the alkane category does not include CH_4. Additionally, the C1-C2 halogens category, dominated by CH_3Cl, was omitted because its contribution was less than 0.2% for both brake types. Labels include MTs for monoterpenes and S-cpds for sulfur-containing compounds. Table S1 and Fig. S8 provide information on the experimental variability across experiments.

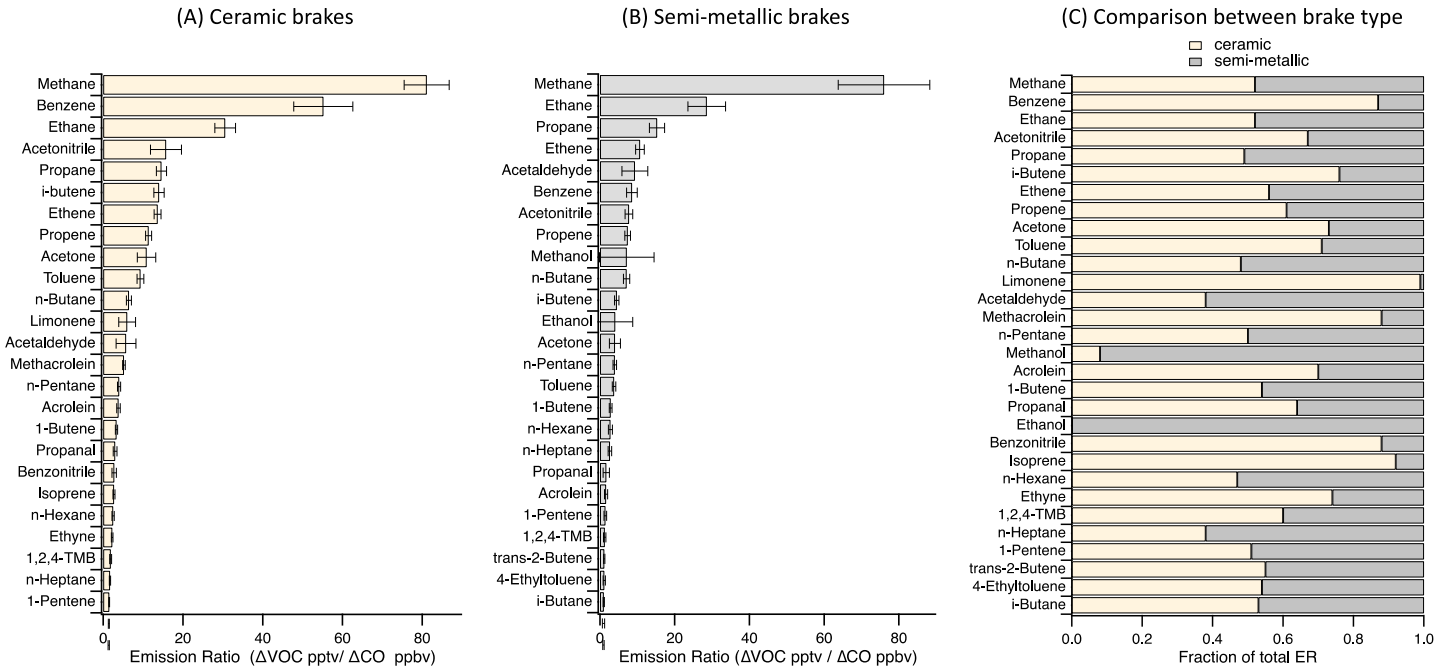
(A) Ceramic brakes
Methane
Benzene
Ethane
Acetonitrile
Propane
i-butene
Ethene
Propene
Acetone
Toluene
n-Butane
Limonene
Acetaldehyde
Methacrolein
n-Pentane
Acrolein
1-Butene
Propanal
Benzonitrile
Isoprene
n-Hexane
Ethyne
1,2,4-TMB
n-Heptane
1-Pentene
0 20 40 60 80
Emission Ratio (ΔVOC pptv/ ΔCO ppbv)
(B) Semi-metallic brakes
Methane
Ethane
Propane
Ethene
Acetaldehyde
Benzene
Acetonitrile
Propene
Methanol
n-Butane
i-Butene
Ethanol
Acetone
n-Pentane
Toluene
1-Butene
n-Hexane
n-Heptane
Propanal
Acrolein
1-Pentene
1,2,4-TMB
trans-2-Butene
4-Ethyltoluene
i-Butane
0 20 40 60 80
Emission Ratio (ΔVOC pptv / ΔCO ppbv)
(C) Comparison between brake type
ceramic
semi-metallic
Methane
Benzene
Ethane
Acetonitrile
Propane
i-Butene
Ethene
Propene
Acetone
Toluene
n-Butane
Limonene
Acetaldehyde
Methacrolein
n-Pentane
Methanol
Acrolein
1-Butene
Propanal
Ethanol
Benzonitrile
Isoprene
n-Hexane
Ethyne
1,2,4-TMB
n-Heptane
1-Pentene
trans-2-Butene
4-Ethyltoluene
i-Butane
0.0 0.2 0.4 0.6 0.8 1.0
Fraction of total ER

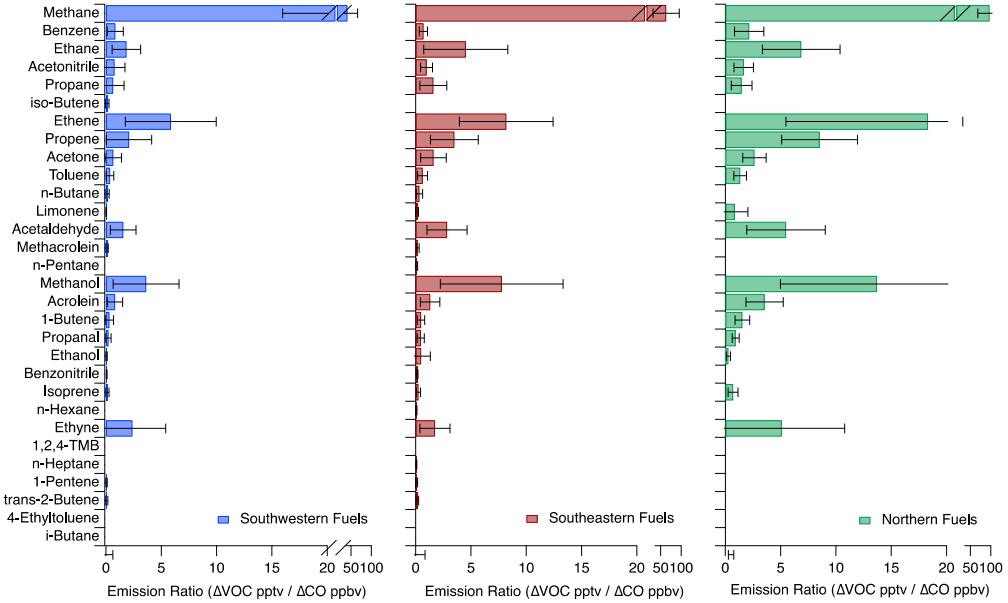
(D) Comparison with biomass burning
Methane
Benzene
Ethane
Acetonitrile
Propane
iso-Butene
Ethene
Propene
Acetone
Toluene
n-Butane
Limonene
Acetaldehyde
Methacrolein
n-Pentane
Methanol
Acrolein
1-Butene
Propanal
Ethanol
Benzonitrile
Isoprene
n-Hexane
Ethyne
1,2,4-TMB
n-Heptane
1-Pentene
trans-2-Butene
4-Ethyltoluene
i-Butane
Southwestern Fuels
Southeastern Fuels
Northern Fuels
0 5 10 15 20 50100
Emission Ratio (ΔVOC pptv / ΔCO ppbv)

Figure 3. Average emission ratios of individual VOC (top 25) relative to CO. Average emission ratios from (A) ceramic brakes and (B) semi-metallic brakes measured using whole air sampling (WAS) collected in regime 2, averaged over six brake dynamometer experiments per brake type and ranked from the most abundant to the least. Error bars for emission ratios represent one standard deviation and are used to determine the corresponding error in relative reactivity. Panel C is a direct comparison between the two brake types. Biomass burning data in panel D were taken from Gilman et al. (2015) and represent laboratory biomass burning studies for combustion of some fuels characteristic of the north (N), southeast (SE) and southwest (SW) regions of the United States.[59] In all panels, TMB stands for trimethylbenzene.

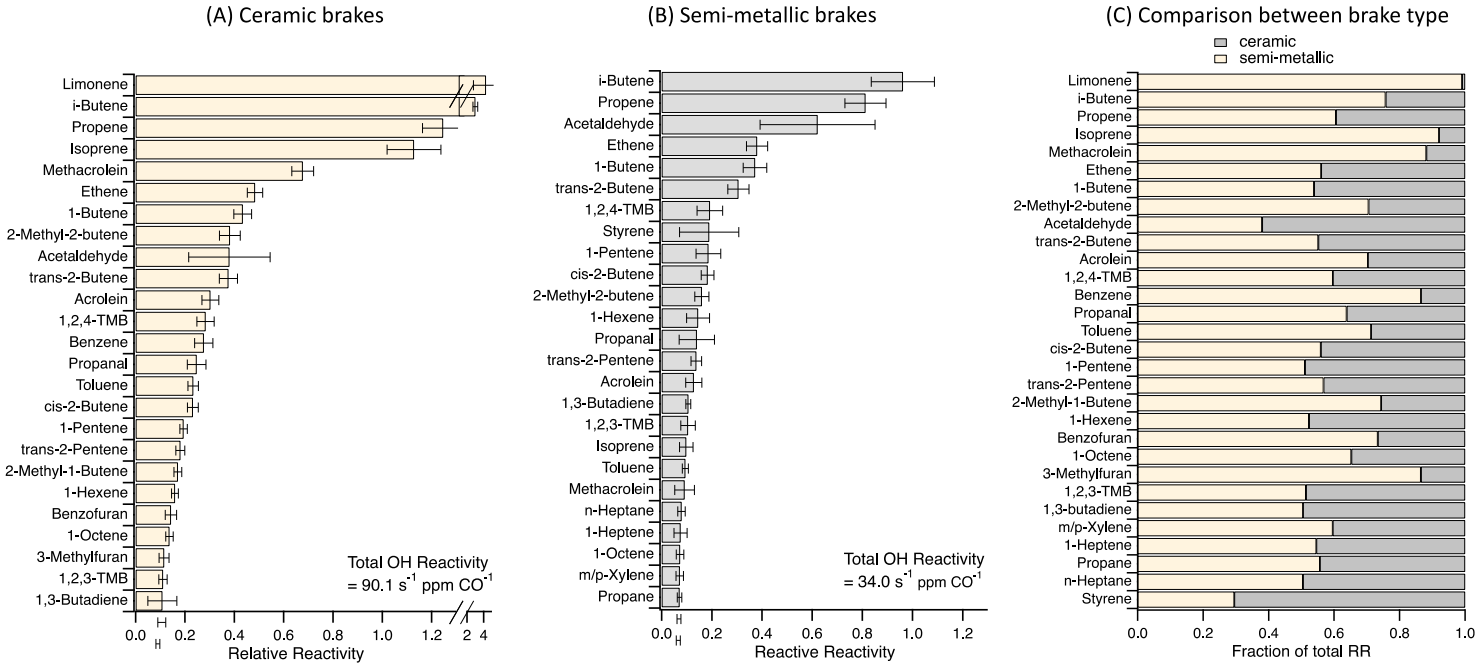
(A) Ceramic brakes
Limonene
i-Butene
Propene
Isoprene
Methacrolein
Ethene
1-Butene
2-Methyl-2-butene
Acetaldehyde
trans-2-Butene
Acrolein
1,2,4-TMB
Benzene
Propanal
Toluene
cis-2-Butene
1-Pentene
trans-2-Pentene
2-Methyl-1-Butene
1-Hexene
Benzofuran
1-Octene
3-Methylfuran
1,2,3-TMB
1,3-Butadiene
Total OH Reactivity
= 90.1 s-1 ppm CO-1
0.0 0.2 0.4 0.6 0.8 1.0 1.2 2 4
Relative Reactivity
(B) Semi-metallic brakes
i-Butene
Propene
Acetaldehyde
Ethene
1-Butene
trans-2-Butene
1,2,4-TMB
Styrene
1-Pentene
cis-2-Butene
2-Methyl-2-butene
1-Hexene
Propanal
trans-2-Pentene
Acrolein
1,3-Butadiene
1,2,3-TMB
Isoprene
Toluene
Methacrolein
n-Heptane
1-Heptene
1-Octene
m/p-Xylene
Propane
Total OH Reactivity
= 34.0 s-1 ppm CO-1
0.0 0.2 0.4 0.6 0.8 1.0 1.2
Reactive Reactivity
(C) Comparison between brake type
ceramic
semi-metallic
Limonene
i-Butene
Propene
Isoprene
Methacrolein
Ethene
1-Butene
2-Methyl-2-butene
Acetaldehyde
trans-2-Butene
Acrolein
1,2,4-TMB
Benzene
Propanal
Toluene
cis-2-Butene
1-Pentene
trans-2-Pentene
2-Methyl-1-Butene
1-Hexene
Benzofuran
1-Octene
3-Methylfuran
1,2,3-TMB
1,3-butadiene
m/p-Xylene
1-Heptene
Propane
n-Heptane
Styrene
0.0 0.2 0.4 0.6 0.8 1.0
Fraction of total RR

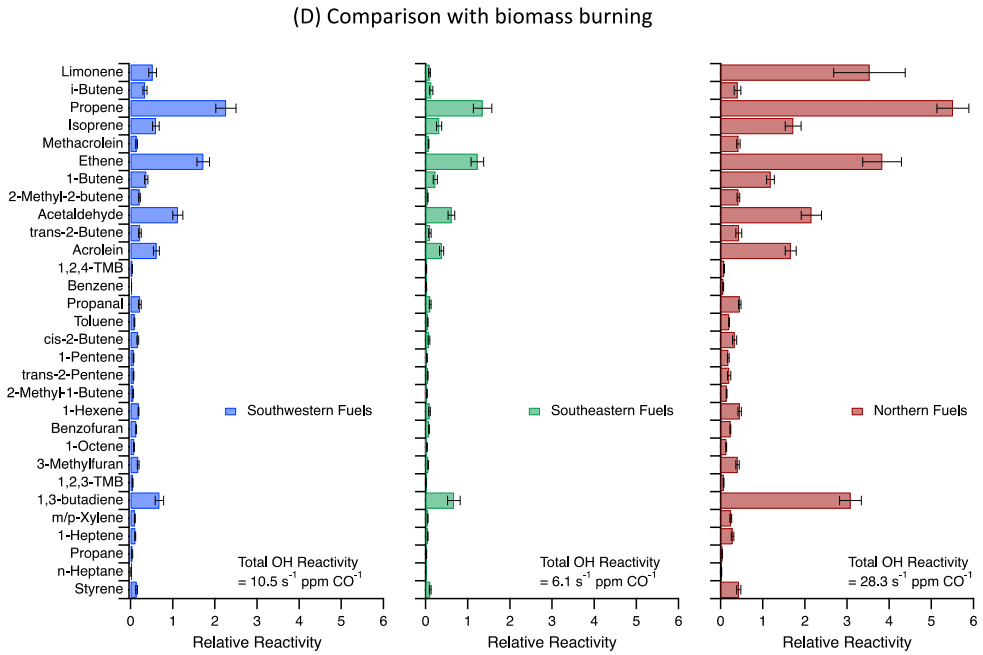
(D) Comparison with biomass burning
Limonene
i-Butene
Propene
Isoprene
Methacrolein
Ethene
1-Butene
2-Methyl-2-butene
Acetaldehyde
trans-2-Butene
Acrolein
1,2,4-TMB
Benzene
Propanal
Toluene
cis-2-Butene
1-Pentene
trans-2-Pentene
2-Methyl-1-Butene
1-Hexene
Benzofuran
1-Octene
3-Methylfuran
1,2,3-TMB
1,3-butadiene
m/p-Xylene
1-Heptene
Propane
n-Heptane
Styrene
Southwestern Fuels
Total OH Reactivity
= 10.5 s-1 ppm CO-1
0 1 2 3 4 5 6
Relative Reactivity
Southeastern Fuels
Total OH Reactivity
= 6.1 s-1 ppm CO-1
0 1 2 3 4 5 6
Relative Reactivity
Northern Fuels
Total OH Reactivity
= 28.3 s-1 ppm CO-1
0 1 2 3 4 5 6
Relative Reactivity

Figure 4. Relative reactivity of individual VOC compounds (top 25) compared to that of CO. Relative reactivity of individual VOC from (A) ceramic brakes and (B) semi-metallic brakes based on emission ratios determined in Fig. 3. Errors bars represent 1 standard deviation calculated from the error in the ER values from Fig. 3, without taking into account the error in the rate constants. Panel C is a direct comparison between the two brake types. TMB stands for trimethylbenzene. For each brake, the total reactivity was calculated similarly to ref. 59 using $total\ OH\ reactivity = \sum(ER \times k_{OH} \times 2.46 \times 10^{10}\ \text{molecules cm}^{-3}\ \text{ppbv}^{-1})$ taking into account the top 25 VOCs listed.

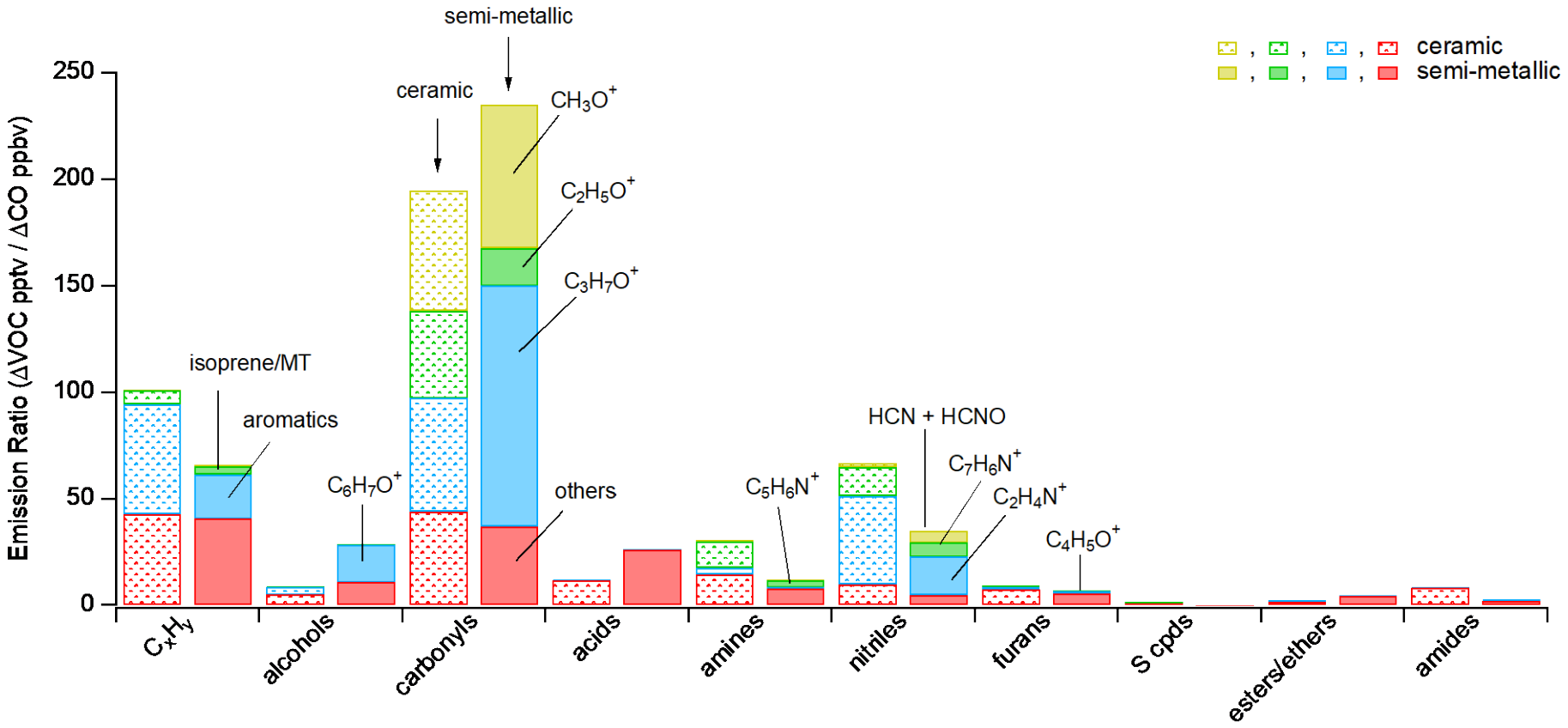

Figure 5. Average emission ratios (ER) of VOC measured with the PTR-MS grouped by functional and structural group class for the ceramic brake (stippled bars) and the semi-metallic brake (solid colored bars). These ER were determined during regime 2 conditions and averaged over six dynamometer experiments per brake type. The C_xH_y category corresponds exclusively to unsubstituted compounds, and substituted VOC with multiple functional groups were counted once in each appropriate functional group category. The contributions from several important VOC with high ER are indicated in separate colors, while the rest of the compounds of a given family are represented in red. NH_3 almost systematically saturated the instrument during regime 2, even with the dilution on, and was excluded from this plot. The contribution from specific brake fluid VOCs (i. e. glycol ethers, see Table S7) was small during these experiments, and to keep the focus strictly on brake emission, these were not included here. Note that some contribution of brake fluid to *m/z* 45 ($C_2H_7O^+$) cannot be excluded.

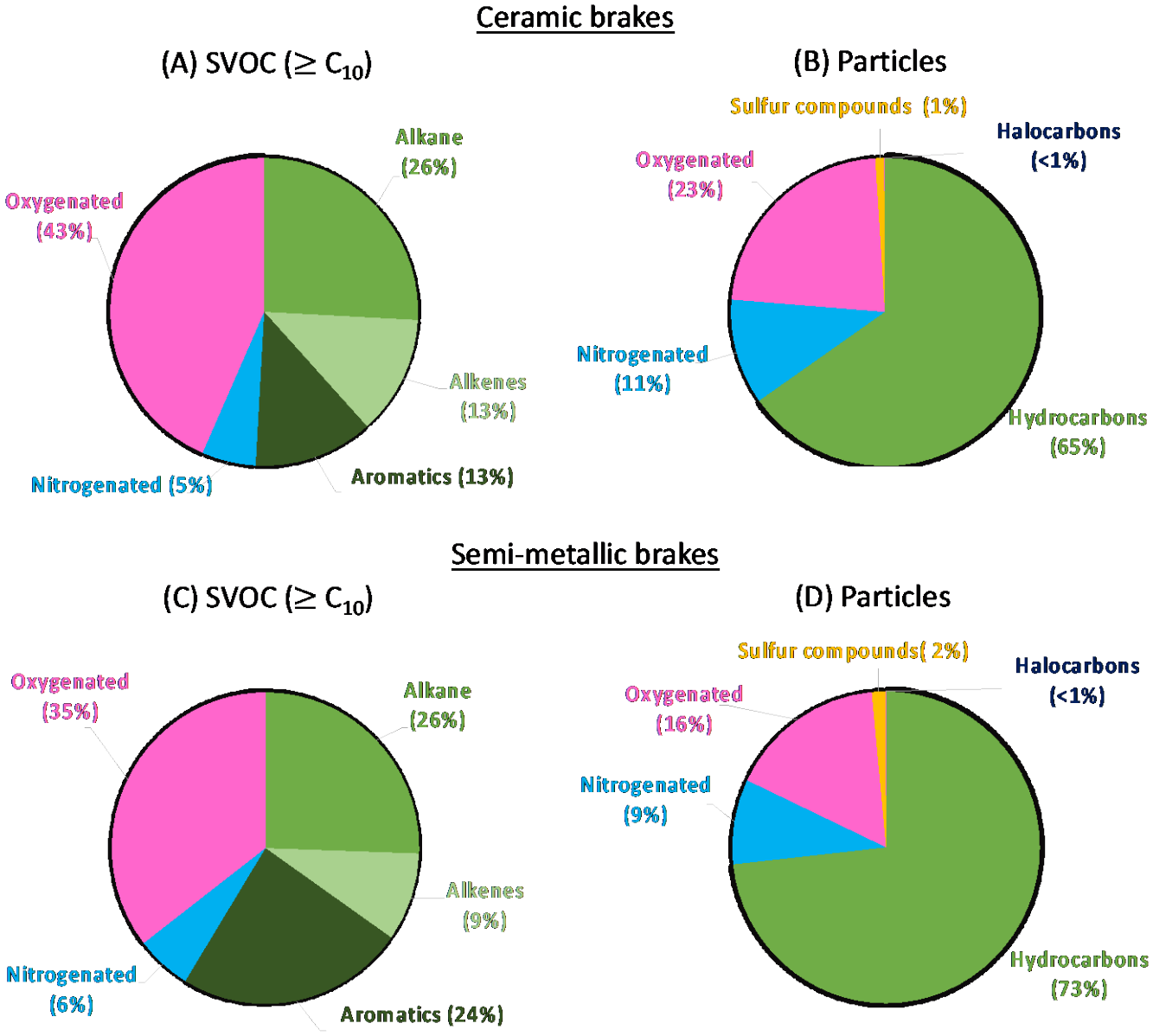

Figure 6. Average semi-volatile organic compound (≥C_{10}) distribution and particle chemical composition measured simultaneously for ceramic or semi-metallic brake pads under heavy braking conditions (regime 2). Mass distributions of (A) SVOC with 10 carbons and more and, (B) particle components for ceramic brakes. Mass distributions of (C) SVOC with 10 carbons and more and (D) particle components for semi-metallic brakes. The SVOC analyses represent an average of 6 experiments per brake type, while the particle analyses represent an average of 3 experiments. No sulfur-containing compounds identified in the SVOCs category, while in panels (B) and (D), sulfur compounds include $C_xH_yS_z^+$ as well as $HS_xO_y^+$ fragments. No halocarbons were identified in the SVOCs category. Figure S13 shows data for each experiment and the corresponding average.